

Transition to shear jamming in colloidal drop impact

P. Shah^{1,†}, S. Arora^{1,†}, M.M. Driscoll^{1,*}

¹*Department of Physics and Astronomy, Northwestern University*

[†]*These authors contributed equally to this work.*

**corresponding author*

Complex fluids, such as particulate suspensions¹ and polymer solutions², exhibit a variety of exotic flow behaviors, for instance shear thickening and jamming. These behaviours are especially relevant to smart material applications, including body armours³ and soft robots⁴. The nonuniform stresses and free-surface geometry in drop impact systems offer a unique lens for probing these flow properties. Here, we use ultrahigh-speed imaging to study the drop impact of colloidal suspensions over a large range of colloidal volume fractions and drop impact velocities. In addition to observing liquid-like spreading and complete solidification, we capture the fascinating transition between these two phases and delineate these regimes in a state diagram. In the spreading regime, we show that the maximum drop spread scales in an identical manner to a Newtonian fluid. In the solidification regime, we measure the speed of shear fronts moving upward from the impact point and quantify the shear jammed fraction of the drop. Moreover, our observation of the shear jamming response to nonuniform stresses is direct visual evidence for recent findings of localised stress fluctuations^{5,6} and dynamically propagating jamming fronts^{7–11}.

An extensive understanding has been developed for the dynamics of a Newtonian fluid drop impacting a dry solid substrate¹². However, the non-Newtonian rheology of complex fluids substantially modifies impact dynamics. Studies have explored the spreading and splashing of a variety of complex fluids^{13–20}, but each has largely focused on a relatively narrow slice of the vast parameter space — for example, a particular range of suspension volume fractions. Here, we report a systematic study of colloidal suspension impact spanning a wide range of colloidal volume fractions ($0.09 \leq \phi \leq 0.50$) and impact velocities ($0.7 \text{ m/s} \leq u_0 \leq 4.0 \text{ m/s}$). We observe fascinating and previously unreported impact behaviours such as localised and partial solidification, and draw connections between these behaviours and the rich flow properties of suspensions.

Rheometry is traditionally used to characterise complex fluids, however this technique only measures flow behavior averaged over the bulk of the fluid. In contrast, our measurements capture the shear jamming transition with a high spatial and temporal resolution. Thus, combined with input from rheological data, our measurements can offer a more holistic understanding of complex fluid flow, particularly at high stresses. In order to connect impact behaviors with flow properties, a mapping between impact velocity and rheological parameters such as shear rate or shear stress is necessary. Due to the nonuniformity of shear in both space and time in drop impact systems, precisely quantifying shear rates is challenging. However, a simple dimensional argument (shear rate $\dot{\gamma} = u_0/d_0$, where d_0 is the initial drop diameter) suggests the shear rate is directly proportional to the impact velocity, u_0 . Thus, by varying the impact velocity, we are able to span the entire range of flow behaviors in these suspensions^{1,21,22}.

For our experiments, we synthesized charge-stabilized silica spheres (diameter 830 ± 20 nm, Fig. 1a) using the Stöber process^{23,24} and suspended them in water. In water, synthesized using the. Spherical drops of diameter $d_0 = 3.0 \pm 0.1$ mm were formed by drawing a known volume of fluid ($15 \mu\text{L}$) into a micropipette. We set the impact velocity by changing the height from which drops were released, and recorded the drops impacting on a dry glass substrate using a high-speed camera. To minimize the effects of particle sedimentation in the samples, all samples were re-suspended immediately before experiments using a vortex mixer. All experiments were performed in a humidity chamber, which additionally mitigated air currents (see Methods for details).

Bulk rheometry measurements [Fig. 1b] demonstrate the variety of flow behaviours exhibited by our suspensions. At low ϕ (black and pink lines in Fig. 1b), the fluid viscosity is constant, akin to a Newtonian fluid. Shear thinning (indicated by decreasing viscosity) becomes pronounced as ϕ is increased (green and purple curves), and shear thickening (indicated by increasing viscosity) appears for $\phi \geq 0.47$ at high shear stresses (orange, blue, and red curves). The inset in Fig. 1b shows the same data plotted as shear stress vs. shear rate, with the dashed line indicating the shear rate ($\dot{\gamma} = u_0/d_0$) corresponding to $u_0 = 2.0$ m/s. It is evident from the inset that at $\phi \geq 0.49$, this impact velocity is sufficient to observe shear thickening (vertical slope of blue and red lines). We note that for lower ϕ , measurements at higher shear stresses were not possible, as the required shear rates were inaccessible by our rheometer (grey triangle at bottom right).

In our drop impact experiments, we observe striking consequences of non-Newtonian flow. In Fig. 1c, we observe patches of localised solidification during spreading — panel 3 of the time-

series shows small solid-like bumps that protrude from the spreading drop, but vanish in panels 4 and 5 [SI video 1]. We also observe partial solidification of the drop — Panel 2 in Fig. 1d shows that the bottom part of the drop acts as a solid, while the top part remains fluid and flows over the solidified region throughout panels 3-4 [SI video 2]. These solidification behaviours are a direct consequence of shear jamming²⁵, evidenced by their occurrence much below the standard jamming threshold ($\phi = 0.55$ for silica spheres²⁶).

To quantify this range of impact outcomes, we computed the normalized maximum diameter of the impacted drops, d_{max}/d_0 , and plotted this metric as a function of u_0 over the whole range of volume fractions [Fig. 2a]. For $\phi \leq 0.47$, d_{max}/d_0 increases with increasing impact velocity. The most striking feature of Fig. 2a, however, is that d_{max}/d_0 drops to 1 at $\phi \geq 0.49$ and high impact velocities. This is because the drop no longer spreads after impact (lower inset). This result is consistent with recent studies that observed similar solidification in dense suspension impact^{15,18}. Our drops remained solid for a few milliseconds; however they spread like a liquid over the timescale of a second [SI video 3]. Thus, the solid-like state we observe is transient in nature, further evidence that this solidification is a direct result of shear jamming. A recent result suggests that the substrate wettability affects this timescale of unjamming¹⁸, but this problem remains largely unexplored.

At $\phi \leq 0.47$, the drops spread in a manner qualitatively similar to Newtonian fluids [SI video 4]. Previous experiments²⁷ with Newtonian fluids have shown d_{max}/d_0 scales as the dimensionless parameter $ReWe^{1/2}$, where Re is the impact Reynolds number ($\rho u_0 d_0 / \eta$, where ρ is the fluid

density and η is the fluid viscosity) and We is the Weber number ($\rho u_0^2 d_0 / \sigma$, where σ is the fluid surface tension). For the impact of colloidal drops, the calculation for the Weber number remains identical to Newtonian fluids; here we used the suspension density computed for each volume fraction, and the surface tension of the suspending fluid. Estimating the Reynolds number is less straightforward, as in the non-Newtonian regime, the fluid viscosity is a function of the continuously changing shear rate. Immediately after impact, the shear rate experienced by the drop is at its maximum ($\dot{\gamma} = u_0 / d_0$). As the fluid spreads and slows down, the shear rate continuously drops to zero. We used the average of the two extremes as the simplest estimate of shear rate throughout the spreading process, $\dot{\gamma}_{avg} = u_0 / 2d_0$. We then used the viscosity value at $\dot{\gamma}_{avg}$ from our rheological data to calculate the effective Reynolds number, Re_{eff} at each ϕ and u_0 . In Fig. 2b, we plot d_{max}/d_0 in the spreading regime against $Re_{eff} We^{1/2}$; the dashed black line indicates the power-law fit, $d_{max}/d_0 = 0.81(Re We^{1/2})^{0.164}$. The exponent of this fit shows excellent agreement with that reported by Scheller et al.²⁷, $d_{max}/d_0 \sim (Re We^{1/2})^{0.166}$. Thus, our simple estimate of shear rates and in turn effective viscosity, provides a useful framework to quantify the maximum spread of colloidal drops, even well into the shear thinning regime. However, for $\phi > 0.47$ where shear thickening is pronounced, this framework no longer holds as the drop does not spread.

We encapsulated the broad range of impact outcomes in a $\phi - u_0$ state diagram [Fig. 3]. Green circles, indicating simple spreading [SI video 4], dominate the low volume fraction and low-shear region. At $\phi = 0.47$, we observe the first consequence of non-Newtonian behavior in the form of pockets of localized solidification that emerge and quickly disappear over milliseconds [SI video 1], indicated by orange diamonds. This regime coincides with the first appearance of shear

thickening in the rheology data [orange curve in Figure 1b]. At even higher ϕ , where rheological measurements show strong shear thickening, we observe a larger and larger fraction of the drop solidifying after impact [SI video 2,3], indicated by blue triangles. The transition between these regimes is a function of both u_0 and ϕ , as all regimes can be accessed by varying either of the parameters while keeping the other constant. Additionally, the drop behavior is very sensitive to small changes in ϕ , consistent with the transition to shear thickening in rheological measurements¹.

The localised solidification regime [orange diamonds in Fig. 3, SI video 1] is especially noteworthy, as solidified patches appear while the bulk of the drop still spreads like a Newtonian fluid [Fig. 2b]. This points to the presence of transient regions of high viscosity embedded in a lower-viscosity fluid phase. Rheological studies using spatiotemporally resolved stress measurements have reported finite regions of enhanced stress in silica suspensions^{5,6}. In these works, Rathee et al.^{5,6} argued that the transition from shear thickening to shear jamming is governed by the growing size of localised shear jammed regions. Our observations of localized solidification are striking visual evidence of such a mechanism. Further spatially resolved stress measurements²⁸ performed on impacting drops could shed more light on the effect of varying external shear in such systems.

For $\phi \geq 0.49$, we observe an increasing fraction of the drop solidifying upon impact. In this regime, we observe a depression at the apex of the drop [Fig. 4a]. We note that this behaviour is not a result of elastic buckling. Instead, a portion of the drop is still fluid, apparent from the ripples visible at the top [SI video 5]. For lower shear rates, where the depression is larger, the fluid portion flows over the solidified base of the drop [SI video 2]. We characterized the extent of drop

solidification by measuring the maximum diameter of this fluid-like depression, α . The normalised depression size, α/d_0 , decreases with increasing u_0 [Fig. 4b]. This is due to a larger and larger fraction of the drop exhibiting solid-like behavior with increasing shear. At $\phi = 0.50$ and $u_0 = 4.0$ m/s, we observe no measurable depression. Additionally, at this impact condition, the drop bounces off the substrate with a coefficient of restitution $\epsilon = 0.1$, indicating that a small fraction of the drop's initial kinetic energy remains after complete solidification [SI video 6]. Thus, by measuring the extent of the fluid-like depression, we are able to characterise the transition between the fluid-like and completely solidified phases.

In the bulk solidification regime, our images captured at 100,000 frames per second allow us to directly observe a disturbance travelling upward over hundreds of microseconds [orange and green arrows in Fig. 4c]. To better visualise this front, we subtract successive frames of the image sequence, so that only the parts that change between frames are highlighted [right panel of Fig. 4c, SI video 7]. The location of the front is given by the lower end of the bright edge. The speed of this front, u_{front} , is constant when measured along the drop surface (slope of the line in inset Fig. 4d). As shown in Fig. 4d, u_{front} increases with increasing u_0 , and its value is several times larger than u_0 . In addition to this front that moves along the drop surface, it is likely that a vertically-traveling front moves through the bulk of our drop. Shear-driven fronts have previously been observed in a number of externally driven dense suspension studies^{7–11}. These fronts were also found to travel at a constant speed much faster than the driving speed, similar to our observation. Further work exploring the interplay between surface and bulk jamming fronts would deepen our understanding of shear propagation in complex fluids.

In conclusion, our highly time-resolved drop impact experiments enable us to systematically probe the entire range of suspension flow regimes. The free-surface geometry in this system provides visual information on the effect of nonuniform stresses on colloidal suspensions, otherwise not accessible via bulk measurements. We show that the impact behavior in the spreading regime can be quantitatively explained via an effective viscosity framework, and that the solidification behaviours at high ϕ and u_0 are direct consequences of non-Newtonian rheology. The shear front we observed propagates over hundreds of microseconds, while the timescale for the drop to unjam (revert to liquid-like behaviour in the absence of shear) is on the order of seconds. This multitude of timescales reveals the rich physics underlying this seemingly simple system.

In the future, spatiotemporally resolved stress measurements²⁸ in drop impact systems could provide further insights into the effect of spatially nonuniform shear. Further work to understand the nature of the shear front traveling along the drop could provide valuable insights into the broader problem of bulk and surface front propagation. Elongated particle suspensions are known to exhibit shear jamming for a much broader range of ϕ ^{26,29}. Drop impact of anisotropic suspensions would both enhance the range of state space where shear jamming is observed, and enrich our understanding of the flow of dense suspensions with an additional orientational degree of freedom.

Methods

Colloidal sample preparation

We fabricated silica spheres in our lab using the Stöber^{23,24} synthesis method. The particle size

was determined by the number of feeds: we performed 14 feeds after the initiation of the reaction, resulting in particles with a diameter of 830 ± 20 nm. The reaction mixture was centrifuged and re-suspended in ethanol 3 times; the suspension was then gravity separated to improve monodispersity. The particles were then imaged on the Hitachi S4800 Scanning Electron Microscope [Fig. 1a]. The particle size was characterized by measuring the diameter of a representative sample of 100 particles in ImageJ, and the polydispersity reported is the standard deviation in particle size.

A concentrated stock suspension of the silica spheres was prepared in water (with no surfactant), and the weight fraction was measured by drying 100 μL of the stock suspension. The density of silica (2 g/cm^3) was used to convert weight fractions into volume fractions. Dilutions were then performed to prepare samples of desired volume fractions. The uncertainty in volume fractions reported is 0.5% (0.005) or less, determined by repeated measurements. When not in use, all the sample tubes were sealed using Parafilm and stored in a refrigerator to minimize evaporation and contamination.

Experimental set-up

We used Fisherbrand plain glass slides as the hydrophilic impact substrate. The slides were cleaned using a 2.5M solution of NaOH in ethanol and water to remove organic impurities. A micropipette was used to form colloidal drops. The micropipette was mounted on a vertically moving pipette holder to vary impact velocities. We used 15 μL of fluid to obtain drops of 3.0 ± 0.1 mm diameter. The setup was enclosed in a humidity chamber with the relative humidity maintained between 70–80% using a saturated solution of NaCl in water, and the humidity was monitored in real time during experiments. Before every trial of the impact experiments, a vortex mixer was used to

re-disperse the sample, ensuring that it was consistently well-mixed.

The impacting drops were backlit using a white LED light, and filmed using two high-speed cameras. The first camera, a Phantom V2512, captured the side-view of the impacting drop at 100,000 frames per second. The second camera, a Phantom V640L, filmed at 20,000 fps. It was tilted at an angle of 15° to gather information on how the impact affected the top surface of the drop. The experiment was repeated at least 5 times for each impact condition to ensure reproducibility.

Rheological studies

Stress-controlled rheological measurements were performed on the colloidal samples over $0.09 \leq \phi \leq 0.50$. The measurements were done on a TA Instruments Discovery HR-2 rheometer at room temperature ($\sim 21^\circ\text{C}$) using the cone-plate geometry with 40 mm diameter and a 1° cone angle. The truncation gap was $25\ \mu\text{m}$. We covered the edges of the samples with a microscope immersion oil to minimize evaporation. The samples were pre-sheared to remove effects of shear history.

Data analysis

All high-speed videos were background-divided and analysed using ImageJ. The plots were made using python, and all errors reported are standard deviations over multiple trials. The maximum drop spread d_{max} (maximum depression diameter α) was determined by locating the frame in the impact timeseries where the extent of the spreading drop (liquid-like depression) was the greatest. To calculate the coefficient of restitution, the speed of the drop before impact u_0 , and the speed after rebound, u_f were computed using several frames of the image sequence. The coefficient of

restitution was then computed as $\epsilon = u_f/u_0$.

To calculate the speed of the upward-moving front, the side-view impact videos recorded at 100,000 fps were used. For every frame of the image sequence, the pixel-wise difference between consecutive frames was taken in ImageJ, so that only the elements that changed between consecutive frames (corresponding to the location of the moving front) were highlighted [SI video 7]. This enabled us to locate the jamming front with a time uncertainty of $10 \mu\text{s}$. The images were then adjusted for brightness and contrast to enhance the moving front. The vertical height h_{front} of the disturbance from the impact substrate was measured. As the front mostly travelled horizontally in the first and last 10 frames of the image sequence, these frames were discarded from this analysis. For every high-speed video, the left and right half of the drop were separately analyzed to obtain two datasets for $h_{\text{front}}(t)$. In order to convert h_{front} to the position along the drop surface, $r\theta_{\text{front}}(t)$, we approximated the drop profile as a circle of radius $r = 1.5 \text{ mm}$ (disregarding the slight deviation from spherical shape during front propagation), and used the relation $h_{\text{front}}(t) = r(1 - \cos \theta_{\text{front}}(t))$, such that $\theta_{\text{front}}(0) = 0$ corresponds to the impact point, to obtain the angle $\theta_{\text{front}}(t)$. A line was then fit to the $r\theta_{\text{front}}$ vs. time plots, and the slope, averaged over the two halves of the drop and several movies for each impact condition (see inset in Fig. 4d), was reported as u_{front} with error bars indicating the standard deviation.

Acknowledgements We thank Jeffrey Richards and Xiang Cheng for useful discussions. This work was supported by the National Science Foundation under award number DMR-2004176. This work made use of the EPIC facility of Northwestern University’s NUANCE Center, which has received support from the SHyNE Resource (NSF ECCS-2025633), the IIN, and Northwestern’s MRSEC program (NSF DMR-

1720139). We thank the Richards Lab at Northwestern University for the use of their rheometry facilities.

Competing Interests The authors declare that they have no competing financial interests.

Correspondence Correspondence and requests for materials should be addressed to MMD.

(michelle.driscoll@northwestern.edu).

Author contributions SA contributed to the conception of the work, experimental design, and data acquisition and analysis. PS contributed to data interpretation and analysis and drafted the manuscript. MMD contributed to the conception of the work, data analysis and interpretation, and drafted the manuscript.

1. Stickel, J. J. & Powell, R. L. Fluid mechanics and rheology of dense suspensions. *Annual Review of Fluid Mechanics* **37**, 129–149 (2005).
2. Osswald, T. & Rudolph, N. Polymer rheology. *Carl Hanser, München* (2015).
3. David, N. V., Gao, X.-L. & Zheng, J. Q. Ballistic Resistant Body Armor: Contemporary and Prospective Materials and Related Protection Mechanisms. *Applied Mechanics Reviews* **62** (2009). 050802.
4. Rus, D. & Tolley, M. T. Design, fabrication and control of soft robots. *Nature* **521**, 467–475 (2015).
5. Rathee, V., Blair, D. L. & Urbach, J. S. Localized stress fluctuations drive shear thickening in dense suspensions. *Proceedings of the National Academy of Sciences of the United States of America* **114**, 8740–8745 (2017).
6. Rathee, V., Blair, D. L. & Urbach, J. S. Localized transient jamming in discontinuous shear thickening. *Journal of Rheology* **64**, 299–308 (2020).
7. Waitukaitis, S. R. & Jaeger, H. M. Impact-activated solidification of dense suspensions via dynamic jamming fronts. *Nature* **487**, 205–209 (2012).
8. Han, E., Peters, I. R. & Jaeger, H. M. High-speed ultrasound imaging in dense suspensions reveals impact-activated solidification due to dynamic shear jamming. *Nature communications* **7**, 1–8 (2016).

9. Han, E., Wyart, M., Peters, I. R. & Jaeger, H. M. Shear fronts in shear-thickening suspensions. *Phys. Rev. Fluids* **3**, 073301 (2018).
10. Peters, I. R., Majumdar, S. & Jaeger, H. M. Direct observation of dynamic shear jamming in dense suspensions. *Nature* **532**, 214–217 (2016).
11. Rømcke, O., Peters, I. R. & Hearst, R. J. Getting jammed in all directions: Dynamic shear jamming around a cylinder towed through a dense suspension. *Phys. Rev. Fluids* **6**, 063301 (2021).
12. Josserand, C. & Thoroddsen, S. T. Drop impact on a solid surface. *Annual review of fluid mechanics* **48**, 365–391 (2016).
13. Bergeron, V., Bonn, D., Martin, J. Y. & Vovelle, L. Controlling droplet deposition with polymer additives. *Nature* **405**, 772–775 (2000).
14. Blackwell, B. C., Deetjen, M. E., Gaudio, J. E. & Ewoldt, R. H. Sticking and splashing in yield-stress fluid drop impacts on coated surfaces. *Physics of Fluids* **27**, 043101 (2015).
15. Boyer, F., Sandoval-Nava, E., Snoeijer, J. H., Dijksman, J. F. & Lohse, D. Drop impact of shear thickening liquids. *Physical review fluids* **1**, 013901 (2016).
16. Peters, I. R., Xu, Q. & Jaeger, H. M. Splashing onset in dense suspension droplets. *Physical review letters* **111**, 028301 (2013).
17. Jørgensen, L., Forterre, Y. & Lhuissier, H. Deformation upon impact of a concentrated suspension drop. *Journal of Fluid Mechanics* **896** (2020).

18. Bertola, V. & Haw, M. D. Impact of concentrated colloidal suspension drops on solid surfaces. *Powder Technology* **270**, 412–417 (2015).
19. Thoraval, M.-J. *et al.* Nanoscopic interactions of colloidal particles can suppress millimetre drop splashing. *Soft matter* **17**, 5116–5121 (2021).
20. Kim, G., Kim, W., Lee, S. & Jeon, S. Impact dynamics of a polystyrene suspension droplet on nonwetting surfaces measured using a quartz crystal microresonator and a high-speed camera. *Sensors and Actuators B: Chemical* **288**, 716–720 (2019).
21. Guy, B., Hermes, M. & Poon, W. C. Towards a unified description of the rheology of hard-particle suspensions. *Physical review letters* **115**, 088304 (2015).
22. van der Vaart, K. *et al.* Rheology of concentrated soft and hard-sphere suspensions. *Journal of Rheology* **57**, 1195–1209 (2013).
23. Stöber, W., Fink, A. & Bohn, E. Controlled growth of monodisperse silica spheres in the micron size range. *Journal of colloid and interface science* **26**, 62–69 (1968).
24. Zhang, L. *et al.* Hollow silica spheres: synthesis and mechanical properties. *Langmuir* **25**, 2711–2717 (2009).
25. Bi, D., Zhang, J., Chakraborty, B. & Behringer, R. P. Jamming by shear. *Nature* **480**, 355–358 (2011).
26. James, N. M., Xue, H., Goyal, M. & Jaeger, H. M. Controlling shear jamming in dense suspensions via the particle aspect ratio. *Soft matter* **15**, 3649–3654 (2019).

27. Scheller, B. L. & Bousfield, D. W. Newtonian drop impact with a solid surface. *AIChE Journal* **41**, 1357–1367 (1995).
28. Cheng, X., Sun, T.-P. & Gordillo, L. Drop impact dynamics: Impact force and stress distributions. *Annual Review of Fluid Mechanics* **54**, null (2022).
29. Williams, S. R. & Philipse, A. P. Random packings of spheres and spherocylinders simulated by mechanical contraction. *Phys. Rev. E* **67**, 051301 (2003).

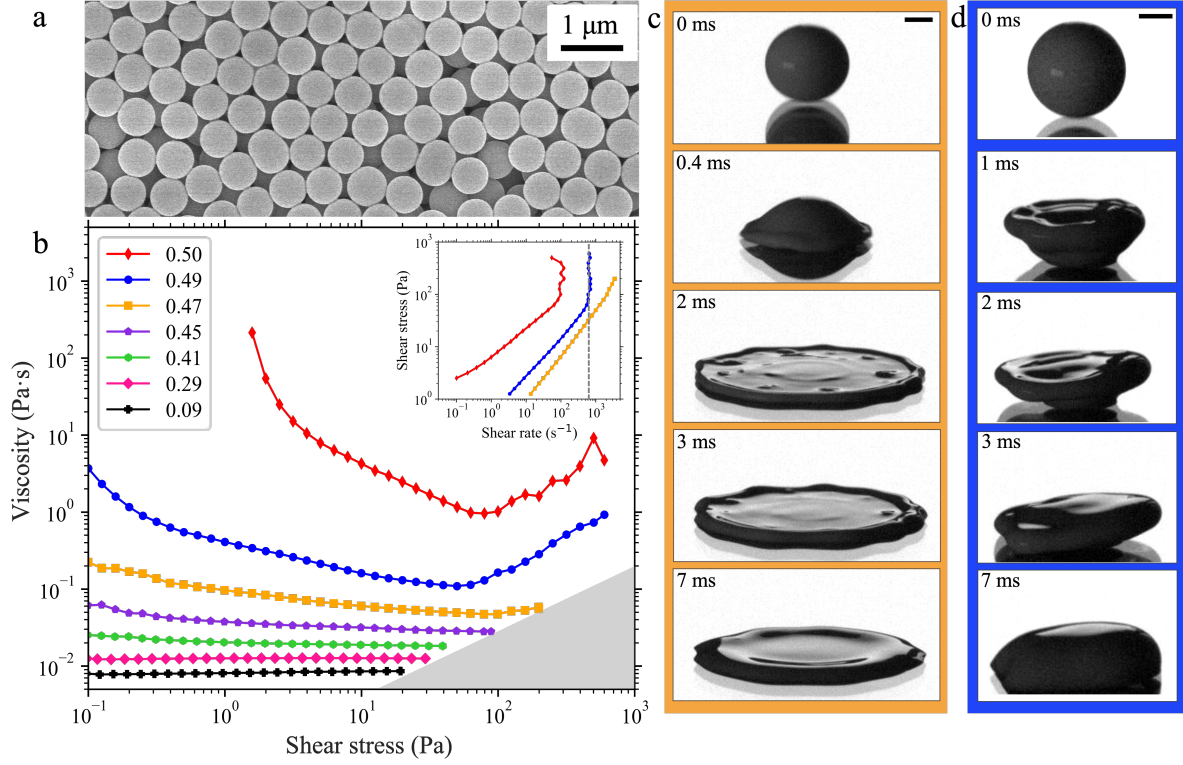


Figure 1: Colloidal system and its exotic impact behaviours. **a** SEM image of the colloidal silica spheres used in our drop impact experiments; the sphere diameter is 830 ± 20 nm. **b** Bulk rheological flow curves: the colloidal suspension exhibits viscous flow, shear thinning, and shear thickening as ϕ is increased. Grey triangle in the bottom right indicates the rate limit of the rheometer. Inset: Shear stress vs. shear rate plotted for $\phi \geq 0.47$. Dashed vertical line denotes the shear rate corresponding to $u_0 = 2.0$ m/s. This shear rate is sufficient for shear thickening, as evidenced by the vertical slope of the stress vs. shear rate curves for $\phi \geq 0.49$. **c** Timeseries of a $\phi = 0.47$ colloidal drop expanding after impacting at $u_0 = 3.0$ m/s [see also SI video 1]. The spreading drop shows transient pockets of localized solidification, indicating the onset of shear jamming. **d** Timeseries of a $\phi = 0.49$ colloidal drop impacting at $u_0 = 2.0$ m/s [see also SI video 2]. The bottom half of the drop solidifies, while the still-fluid top portion flows over it. Scale bars are 1 mm in c and d.

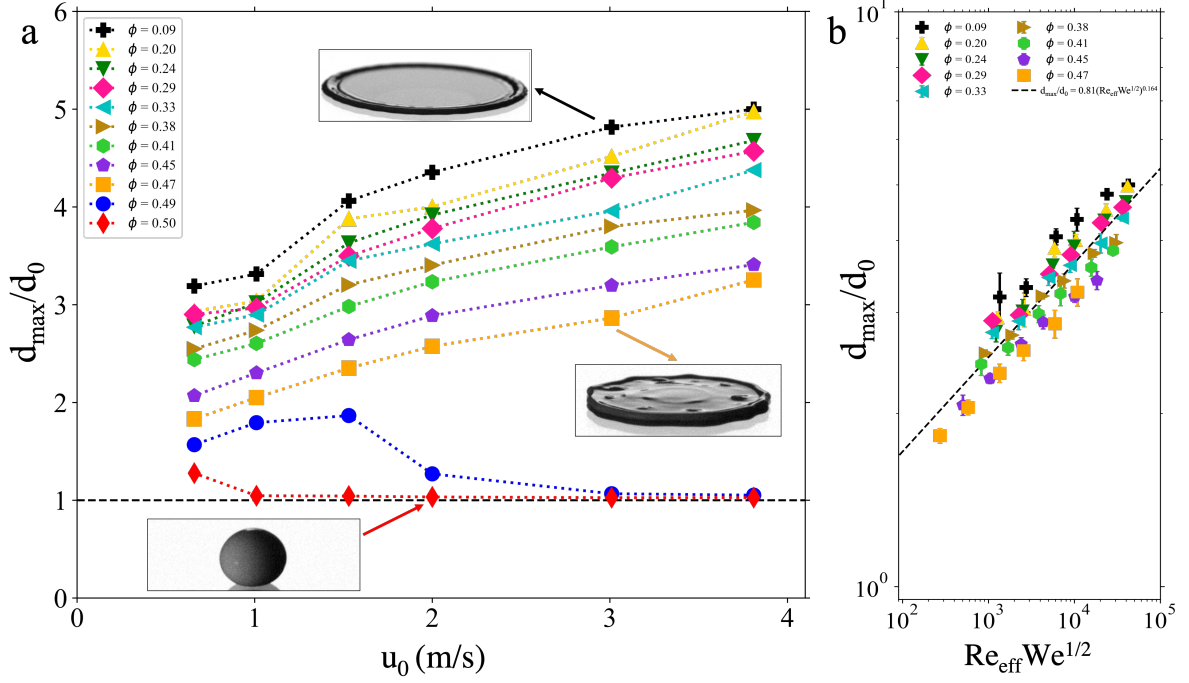


Figure 2: **Quantifying post-impact spreading.** **a** Normalised maximum diameter, d_{max}/d_0 , as a function of u_0 for various volume fractions ϕ . For $\phi \geq 0.49$ and high impact velocities, d_{max}/d_0 drops to 1, indicating the drop does not spread. Insets show representative snapshots of simple spreading (upper), localised solidification (middle), and bulk solidification (lower). Dotted lines are guides to the eye, and the dashed black line indicates $d_{max}/d_0 = 1$. **b** Normalised maximum diameter, d_{max}/d_0 , for $\phi \leq 0.47$ plotted against the dimensionless parameter $Re_{eff} We^{1/2}$. The exponent of the power law fit (dashed line, $d_{max}/d_0 = 0.81(Re_{eff} We^{1/2})^{0.164}$) is in excellent agreement with the scaling reported for Newtonian fluids²⁷.

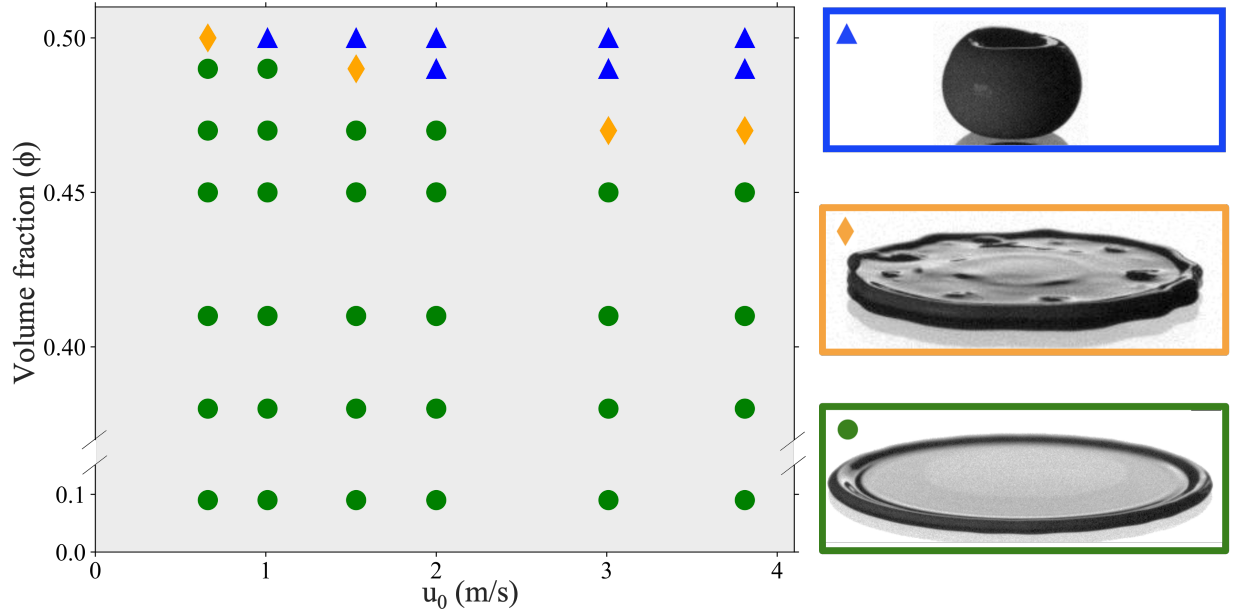


Figure 3: **State diagram of colloidal drop impact.** $\phi - u_0$ state diagram summarizing impact regimes; representative snapshots corresponding to these regimes are shown on the right. Green circles denote simple spreading behavior, which dominates the low ϕ , low u_0 region. Orange diamonds indicate that transient pockets of localised solidification were observed during spreading. Blue triangles correspond to the partial/full solidification regime, where the bottom portion of the drop jams after impact, but a shrinking region at the top remains fluid.

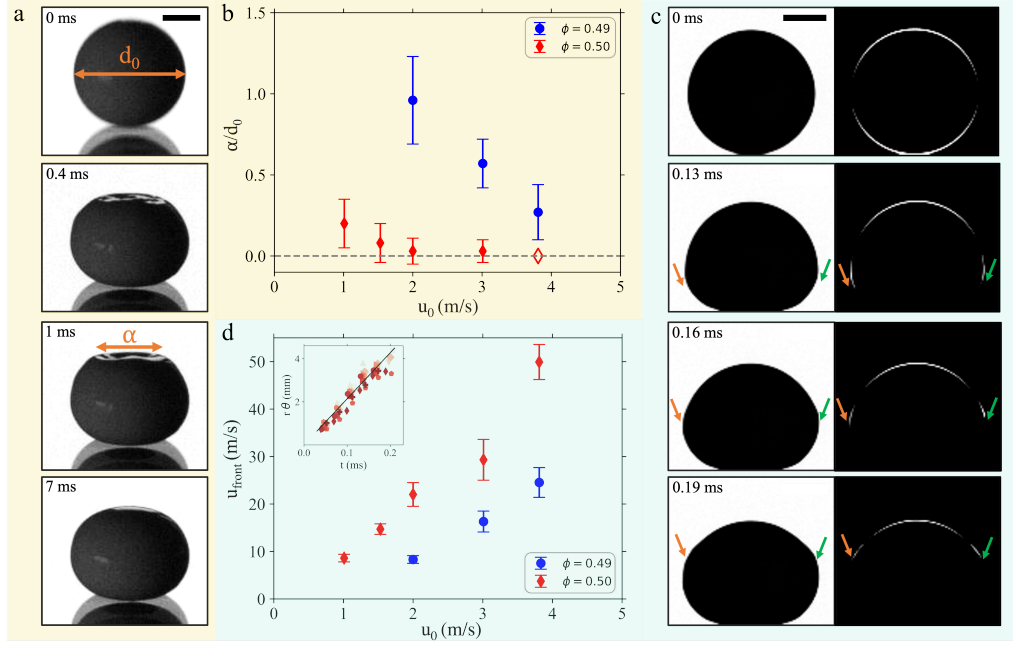


Figure 4: **Characterisation of the partial solidification regime.** **a** Timeseries of a $\phi = 0.49$ drop impacting at $u_0 = 3.0$ m/s [see also SI video 5], where much of the drop solidifies at impact, but a liquid-like depression of maximum width α is observed at the apex; scale bar is 1 mm. **b** The normalised maximum width of the fluid-like depression, α/d_0 , vs. impact velocity. α/d_0 decreases with increasing impact velocity, indicating that an increasing portion of the drop is in the solid-like phase. Hollow diamond denotes the absence of a measurable depression. **c** Timeseries of a $\phi = 0.50$ drop impacting at $u_0 = 2.0$ m/s [see also SI video 7]. Right panels show images obtained by subtracting consecutive frames, so that the edge of the solidification front is highlighted. The arrows highlight the front moving along the drop surface; the left and right halves of the drop were analysed separately. Scale bar is 1 mm. **d** The speed of the shear front measured along the drop surface, u_{front} , vs. impact velocity u_0 . u_{front} is several times larger than u_0 . Inset: position of the front, $r\theta$, vs. time for 12 datasets at $\phi = 0.50$ and $u_0 = 2.0$ m/s; slope of the solid black line is

u_{front} .